HHS Public Access

Author manuscript

Magn Reson Med. Author manuscript; available in PMC 2021 April 01.

Published in final edited form as:

Magn Reson Med. 2020 April ; 83(4): 1512–1518. doi:10.1002/mrm.28005.

A dual-tuned $^{17}O/^{1}H$ head array for direct brain oximetry at 3 Tesla

Karthik Lakshmanan[1,2,*], **Seena Dehkharghani**[1], **Guillaume Madelin**[1,2,3], **Ryan Brown**[1,2,3]

[1]Bernard and Irene Schwartz Center for Biomedical Imaging, Department of Radiology, New York University School of Medicine, New York, NY, USA

[2]Center for Advanced Imaging Innovation and Research (CAI2R), Department of Radiology, New York University School of Medicine, New York, NY, USA

[3]The Sackler Institute of Graduate Biomedical Science, New York University School of Medicine, New York, NY, USA

Abstract

Purpose: To design and build a dual-tuned $^{17}O/^{1}H$ coil for direct brain oximetry at 3 T

Methods: A dual tuned $^{17}O/^{1}H$ coil comprising two degenerate mode birdcage coils was constructed to facilitate high sensitivity ^{17}O and ^{1}H imaging. *In vivo* ^{17}O brain images were acquired in a healthy volunteer using a FLORET sequence, together with high-resolution structural brain ^{1}H anatomic imaging.

Results: Natural abundance ^{17}O images with a nominal resolution of 8 mm^3 were acquired in under 20 minutes exhibiting clear delineation of the physiologic ^{17}O distribution. 1 mm isotropic ^{1}H structural brain images demonstrated excellent quality and anatomic detail using routine clinical imaging sequence parameters and parallel acceleration.

Conclusion: A dual tuned $^{17}O/^{1}H$ array was constructed to enable high sensitivity ^{17}O and ^{1}H imaging under standard clinical 3 T scanning conditions.

Keywords

magnetic resonance imaging; oxygen-17; oximetry; brain

Introduction

Brain homeostasis depends critically upon the steady nutritive flow of oxygenated blood, hinging on the immense energetic advantage of oxidative phosphorylation to sustain the neurovascular unit at rest and during explicit activation. Seminal paradigms of sequential hemodynamic compromise have been expounded using ^{15}O PET, emphasizing a tenuous state of so-called misery perfusion, marked by impaired oxygen metabolism and conferring elevated near-term stroke risk[1,2,3]. The development of ^{15}O translational and clinical

*Corresponding Author: Karthik Lakshmanan, Bernard and Irene Schwartz Center for Biomedical Imaging, New York University School of Medicine, 660 First Avenue, Room 401, New York, NY 10016, Tel: 212-263-1170, Fax: 212-263-7541, Karthik.lakshmanan@nyumc.org.

imaging programs, however, proves challenging due to the reliance upon short lived radiotracers (half-life ~90 s) and the dependence upon in situ cyclotron access for in vivo experimentation. Indirect approaches to assessing oxygen metabolism using ^{1}H MRI have therefore been proposed to circumvent the technical obstacles associated with ^{15}O [4–8], but require complex biophysical modeling and suffer generally poor anatomic localization. Direct MR oximetry, exploiting the stable and naturally occurring ^{17}O isotope has been explored in human and non-human species; however, its low natural abundance (0.037%) has demanded ultrahigh field MR systems (> 3 T) coupled to fractionally enriched ^{17}O gas inhalation, limiting widespread translational or clinical applicability [9–15].

While sporadic reports of ^{17}O oximetry at 3 T exist[16], the widespread adoption of ^{17}O MRI beyond purely translational applications requires specialized dual-tuned RF coils to enable concurrent ^{1}H imaging for comprehensive, real-time multi-parametric structural, functional, metabolic, and hemodynamic interrogation of the living brain. In this work we developed a dual-tuned ^{17}O/^{1}H coil array to explore the feasibility of natural abundance brain oximetry on a clinical 3 Tesla system, emphasizing high ^{17}O-MRI sensitivity, ^{1}H-MRI performance, and engineering features which could potentially support future simultaneous co-modal, multi-parametric brain PET-MR imaging.

Methods

Design Approach

Given the low natural abundance of ^{17}O, our top design objective was to engineer a coil array with optimal ^{17}O performance while still maintaining clinically acceptable ^{1}H sensitivity, ensuring the full battery of neurovascular proton MRI techniques.

Recent work has shown that dual-nucleus degenerate mode birdcage arrays[17,18] can be arranged to achieve improved X-nucleus and ^{1}H performance over dual-tuned birdcage coils. Following this strategy, we built two radially interleaved degenerate mode birdcages that integrated four ^{17}O (16.7 MHz) and eight ^{1}H (123.2 MHz) channels (Fig. 1). The ^{17}O unit was required to operate in transmit/receive (Tx/Rx) mode due to the lack of a commercially available coil. The ^{1}H unit was designed as a Rx-only phased array to enable the system body coil for ^{1}H excitation, facilitating applications such as spin labelling that require cervical RF tagging beyond the coverage of the local coil.

To reduce PET attenuation, we consolidated the arrays into a two “layer” structure (layer 1 is the ^{17}O Tx/Rx array and layer 2 is the ^{1}H Rx array), moved interface components such as the preamplifiers, Tx/Rx switches, and power dividers, and majority of tuning capacitors outside the FOV that extends radially outward from the brain, and enclosed the device in a 3D printed (Fortus 360, Stratasys, Minneapolis) stealth polycarbonate shell. A detailed description of the two arrays is provided in the following sections.

^{17}O Array

Given the low operating frequency of ^{17}O (16.7 MHz) the coil array design had to be chosen to achieve a balance between the high peripheral SNR of a high channel array and high central SNR of a low channel array. To select the number of coils in the ^{17}O array, we built

test coils with 45° and 90° apertures to emulate individual coils in eight and four channel arrays, respectively. The coils were built on a head-sized domed substrate that was 27 cm long. We measured the unloaded and loaded quality factor (Q) in three cases: 1) 90° aperture coil with two distributed capacitors, 2) 90° aperture coil with four distributed capacitors, and 3) 45° aperture coil with two distributed capacitors. The loaded Q measurements were made on a tissue equivalent head phantom[19]. Of the candidates tested, we found that the 90° aperture coil with two distributed capacitors had the highest unloaded Q and unloaded-to-loaded Q ratio (Table 1). Additionally, previous work[17] suggests that a low-frequency, eight-channel array that encircles the head can be expected to exhibit significant coupling between third and fourth neighbors, which can be complicated to decouple.

We therefore chose to build a four-channel ^{17}O array (Fig. 1) whose coils were distributed with radial symmetry around a head-shaped polycarbonate substrate (20 cm x 33 cm x 27 cm). The ^{17}O coils were constructed with 10 mm wide, 0.06 mm thick copper tape and matched to 50Ω at 16.7 MHz using two distributed capacitors in the presence of the tissue-equivalent head phantom. The perimeter of the ^{17}O coils was 114 cm, potentially long enough to support standing waves at the ^{1}H frequency (123.2 MHz). To reduce interaction between the ^{1}H and ^{17}O coils, the distributed capacitors in the ^{17}O coils were replaced with lumped element second-order filters that were set up to provide high impedance at the ^{1}H frequency and the appropriate capacitance to resonate the coil at ^{17}O frequency[20], along with one first-order filter[21] that provided high impedance at the ^{1}H frequency (Fig. 1).

While the coils were set up individually (in other words, without shared rungs), we collapsed the modes to achieve degeneracy by decoupling neighboring elements by geometrical overlap and the next nearest neighbors by linked counter-wound inductors (Fig. 1). Scattering (S) parameters were measured to determine decoupling efficacy. The ^{17}O array was interfaced to the system's broadband power amplifier through a one-to-four way power splitter. To achieve circularly polarized transmit excitation, home-built lumped element phase shift networks were added to provide 90^{o} phase offsets based on the azimuthal location of the coil elements. Individual power splitter outputs were connected to Tx/Rx switches[22] to isolate and protect the preamplifiers during ^{17}O excitation (Fig. 1). The coil ground was separated from the common system ground by two cable traps, one tuned to ^{17}O and the other tuned to ^{1}H frequency. Preamplifier decoupling was achieved by adding a phase shift network in the receive path that transformed the low input impedance of the preamplifier into an inductance that formed a parallel resonant circuit with the match capacitor[23].

^{1}H Array

The ^{1}H unit was a degenerate mode birdcage with 8-channels in which neighboring coils have shared rungs. In the past, degenerate mode birdcages have been utilized when both a uniform excitation field and phased array signal reception are desired[24,25]. In this case, we used the concept in Rx only mode in order to reduce the copper footprint and therefore the PET attenuation compared to an overlapped array. The coils were laid out with radial symmetry around the substrate using 5 mm wide, 0.06 mm thick copper tape to circumscribe loops that were 24 cm long with 45° apertures (12 cm arc length). The coils were tuned to

123.2 MHz using six distributed capacitors and matched to 50Ω in the presence of the head phantom. The ratio between the shared rung and end ring capacitors was chosen to decouple nearest neighbor coils. Next nearest neighbor decoupling was addressed using preamplifier decoupling. The coil Q values were approximately 310 (unloaded) and 85 (loaded).

Spin excitation was produced by system body coil. To isolate the receive array and to ensure patient safety during body coil operation one active detuning circuit and one current fuse rated at 700 mA were integrated per ^{1}H coil.

MRI and PET Measurements

All imaging experiments were performed on Siemens 3 T Prisma scanner (Siemens Healthineers, Erlangen, Germany). Human subjects were scanned after obtaining their informed written consent. ^{1}H and MNO “TIM to 4G” adapter interfaces (Siemens Healthineers, Erlangen, Germany) were used to route the received ^{1}H and ^{17}O signals from the array to the respective receive chains. The ^{17}O transmit power was restricted to enforce a two-fold safety buffer below the 10 W/kg limit set by the International Electrotechnical Commission (IEC document 60601–2-33 2010).

^{1}H Flip angle maps were measured in the head phantom with and without the ^{17}O/^{1}H array to ensure the integrity of the ^{1}H transmit field produced by the system body coil was preserved.

The ^{17}O reference pulse amplitude to generate a 90º flip angle was determined by recording the maximum signal amplitude acquired with a Stimulated Echo Acquisition Mode (STEAM)[26] sequence (TE=20ms, TR= 2000ms, TM = 10 ms, BW =1200 Hz, Ave = 16) for a range of pulses (200 to 300 V in steps of 20 V). In vivo ^{17}O-MRI was demonstrated using a three-dimensional non-Cartesian Fermat Looped Orthogonally Encoded Trajectories (FLORET) [27,28] acquisition with the following parameters: TR = 50 ms, TE = 0.2 ms, flip angle = 90°, resolution = 8 mm isotropic, 3 hubs at 45º, 140 interleaves/hub, field of view = 512 mm isotropic, 56 averages, readout time = 10.3 ms, acquisition time = 19:36 min.

^{1}H SNR and flip angle measurements were performed with the developed array and a product commercial phased array (Head/Neck 20, Siemens Healthineers, Erlangen, Germany, and (23cm x 38 cm x 27 cm) available at our center. The commercial array has twenty coils arranged in three rows along the Z direction of 8, 8, and 4 coils. The final row of 4 coils is used for neck imaging and was disabled in our measurements. SNR maps were calculated from separate signal and noise (with the RF pulse amplitude set to zero) measurements acquired with a gradient echo pulse sequence and processed with the optimal array combination method[29]. The SNR acquisition parameters were as follows: TR = 500 ms, TE = 3.82 ms, flip angle = 10°, voxel size = 0.9×0.9×3 mm^{3}. The ^{1}H flip angle maps were measured using the method described in Ref[30]. Proton anatomical imaging was performed with a magnetization-prepared rapid acquisition gradient echo (MPRAGE) sequence: TR = 2200 ms, TE = 3.2 ms, TI = 900 ms, flip angle = 8°, resolution = 1 mm isotropic, parallel acceleration factor = 2, and acquisition time = 4:30 min.

To measure the influence of the MRI coils on 511 keV photons, we recorded the true net counts over 5 minute intervals that were emitted from a 5.4 L water phantom doped with 1.14 miC ^{18}F-FDG in three environments on a 3T PET-MR system (Biograph mMR, Siemens Healthineers, Erlangen Germany): 1) no local coil present (reference), 2) inside the ^{17}O/^{1}H array, and 3) inside the commercial head/neck PET coil (mMR head array, Siemens Healthineers, Erlangen, Germany). The value recorded in the reference environment was used to predict the net counts in subsequent measurements while accounting for FDG decay. The attenuation loss from the coils is reported as the ratio between the actual and predicted true net counts.

Results

^{17}O Array

For the ^{17}O coils, the average S-parameter reflection was −15 dB and the average isolation was −14 dB and −18 dB between neighbors and next nearest neighbors, respectively. The worst isolation between neighbor and next nearest neighbors were −13.6 and −17.4 dB respectively. The insertion loss of the ^{17}O power dividers and Tx/Rx switches was - 0.3 ± 0.1 dB with 90º ± 1º phase intervals at each output. A ^{17}O transmit pulse with 240 V amplitude and 500 μs duration produced a 90º flip angle. Orthogonal ^{17}O images acquired with an isotropic 3D FLORET sequence in a healthy adult volunteer (Fig. 2 top row) demonstrate the feasibility of direct oximetry under natural abundance conditions without enrichment. Anatomical delineation of the cerebral hemispheres and substructure is apparent at the current spatial resolution.

^{1}H Array

For the ^{1}H coils, the average S-parameter reflection was −15 dB and the average isolation was −9 dB and −11 dB between neighbors and next nearest neighbors, respectively. The worst isolation was −8.4 dB and −10.6 dB between neighbors and next nearest neighbors respectively. The system body coil required a 202 V, 500 μs hard pulse to achieve 90º flip angle when the array was present and 188 V when the array was absent. ^{1}H flip angle maps acquired with and without the ^{17}O/^{1}H array (Fig. 3) show that it caused minimal distortion to the transmit field produced by the system body coil. ^{1}H SNR at the center of the head phantom was 20% lower when compared to the commercial Head/Neck 20 array (Fig. 4). Concurrent multi-planar reconstructions from an MPRAGE sequence obtained in the same imaging session (Fig. 2 Bottom row) confirm the suitable performance of the ^{1}H array, exhibiting high anatomic detail and tissue contrast at isotropic 1 mm resolution.

PET

The commercial mMR head array attenuated 15.1% of the net true photon counts from the FDG-doped phantom, while the ^{17}O/^{1}H array attenuated 7.7%, indicating the developed array’s PET compatibility for future co-modal measurements.

Discussion and Conclusions

In this work we developed a dual tuned $^{17}O/^{1}H$ array comprising radially interleaved degenerate mode birdcage coils. The ^{17}O unit operated in Tx/Rx mode to ensure uniform excitation during transmission and high sensitivity during signal reception. The ^{17}O image quality confirms the feasibility of natural abundance oximetry at 3 T[16].

The ^{1}H unit was engineered to support the full battery of neurovascular proton MRI. Hence we chose to build a ^{1}H Rx only array and utilize the system body coil for spin excitation, which represents a departure from most dual-tuned arrays that consist of a pair of local Tx/Rx arrays[17,18,25,31–34].

To preserve the integrity of the ^{1}H excitation field produced by the system body coil we incorporated ^{1}H blocking circuits[20,21] in ^{17}O elements, which caused a reduction in the unloaded to loaded Q ratio (Table 1). Using the well-known relationship between Q ratio and SNR ($SNR = \sqrt{1 - \frac{Ql}{Qun}}$) we can equate this reduction in Q to a SNR penalty of 8%. We chose to implement the blocking circuits to harvest the potential advantages of an Rx only ^{1}H array such as improved excitation coverage and sensitivity over a local ^{1}H transmit array. Eight of the 12 blocking circuits were positioned outside the FOV to improve PET transparency. While a μ-map generated from a high-dose CT scan to enable local coil attenuation correction and simultaneous PET/MR are pending at the time of this report, the PET true photon count measurements showed that the $^{17}O/^{1}H$ array provided ~50% improved PET transparency over the commercial head coil. This result suggests that the $^{17}O/^{1}H$ array is congruent with attenuation correction and co-modal operation.

In conclusion we designed and implemented a multi-channel $^{17}O/^{1}H$ array for direct brain oximetry at 3 T. The array is underpinned with dual degenerate mode birdcages to reduce its electrical component footprint for co-modal PET measurements, a 4-channel ^{17}O receiver to enhance sensitivity, and a receive-only 8-channel ^{1}H array to enable body coil functionality. We anticipate that the head coil will allow a new set of functional, metabolic, and hemodynamic measurements in the brain.

Acknowledgements.

The authors thank Jerzy Walczyk for help with the coil housing and Riccardo Lattanzi for the SNR calculation tool. This work was partially supported by National Institutes of Health grants R01DK106292, R01NS097494, R21CA213169, R01EB026456, R21AG061579, and R01DK114428 and was performed under the rubric of the Center for Advanced Imaging Innovation and Research (CAI2R, www.cai2r.net) at the New York University School of Medicine, which is an NIBIB Biomedical Technology Resource Center (NIH P41 EB017183).

References

1. Derdeyn CP, Carpenter DA, Yundt KD, et al. Variability of cerebral blood volume and oxygen extraction: stages of cerebral haemodynamic impairment revisited. Brain. 2002;125(3):595–607. [PubMed: 11872616]
2. Grubb RL, Powers WJ, Clarke WR, Videen TO, Adams HP, Derdeyn CP. Surgical results of the Carotid Occlusion Surgery Study. 2013;118(1):25.
3. Powers WJ. Cerebral hemodynamics in ischemic cerebrovascular disease. 1991;29(3):231–240.

4. Bolar DS, Rosen BR, Sorensen AG, Adalsteinsson E. QUantitative Imaging of extraction of oxygen and TIssue consumption (QUIXOTIC) using venular-targeted velocity-selective spin labeling. 2011;66(6):1550–1562.
5. Bulte DP, Kelly M, Germuska M, et al. Quantitative measurement of cerebral physiology using respiratory-calibrated MRI. NeuroImage. 2012;60(1):582–591. [PubMed: 22209811]
6. Gauthier CJ, Hoge RD. Magnetic resonance imaging of resting OEF and CMRO2 using a generalized calibration model for hypercapnia and hyperoxia. NeuroImage. 2012;60(2):1212–1225. [PubMed: 22227047]
7. An H, Lin W. Impact of intravascular signal on quantitative measures of cerebral oxygen extraction and blood volume under normo- and hypercapnic conditions using an asymmetric spin echo approach. 2003;50(4):708–716.
8. Zhang J, Zhou D, Nguyen TD, Spincemaille P, Gupta A, Wang Y. Cerebral metabolic rate of oxygen (CMRO2) mapping with hyperventilation challenge using quantitative susceptibility mapping (QSM). 2017;77(5):1762–1773.
9. Zhu XH, Chen W. In vivo oxygen-17 NMR for imaging brain oxygen metabolism at high field. Progress in Nuclear Magnetic Resonance Spectroscopy. 2011;59:319–335. [PubMed: 22027341]
10. Kurzhunov D, Borowiak R, Hass H, et al. Quantification of oxygen metabolic rates in Human brain with dynamic 17O MRI: Profile likelihood analysis. 2017;78(3):1157–1167.
11. Kurzhunov D, Borowiak R, Reisert M, Krafft AJ, Ozen AC, Bock M. 3D $CMRO_2$ mapping in human brain with direct ^{17}O MRI: Comparison of conventional and proton-constrained reconstructions. NeuroImage. 2017;155:612–624. [PubMed: 28527792]
12. Lu M, Zhang Y, Ugurbil K, Chen W, Zhu X-H. In vitro and in vivo studies of 17O NMR sensitivity at 9.4 and 16.4 T. 2013;69(6):1523–1527.
13. Hoffmann SH, Begovatz P, Nagel AM, et al. A measurement setup for direct 17O MRI at 7 T. 2011;66(4):1109–1115.
14. Niesporek SC, Umathum R, Lommen JM, et al. Reproducibility of CMRO2 determination using dynamic 17O MRI. 2018;79(6):2923–2934.
15. Atkinson IC, Thulborn KR. Feasibility of mapping the tissue mass corrected bioscale of cerebral metabolic rate of oxygen consumption using 17-oxygen and 23-sodium MR imaging in a human brain at 9.4 T. Neuroimage. 2010;51(2):723–733. [PubMed: 20188194]
16. Borowiak R, Groebner J, Haas M, Hennig J Bock, MJMRMiP, Biology, Medicine. Direct cerebral and cardiac 17O-MRI at 3 Tesla: initial results at natural abundance. 2014;27(1):95–99.
17. Lakshmanan K, Brown R, Madelin G, Qian Y, Boada F, Wiggins GC. An eight-channel sodium/proton coil for brain MRI at 3 T. NMR in Biomedicine. 2018;31(2):e3867.
18. Brown R, Khegai O, Parasoglou P. Magnetic Resonance Imaging of Phosphocreatine and Determination of BOLD Kinetics in Lower Extremity Muscles using a Dual-Frequency Coil Array. Scientific Reports. 2016;6:30568. [PubMed: 27465636]
19. Ianniello C, de Zwart JA, Duan Q, et al. Synthesized tissue-equivalent dielectric phantoms using salt and polyvinylpyrrolidone solutions. 2018;80(1):413–419.
20. Meyerspeer M, Roig ES, Gruetter R, Magill AW. An improved trap design for decoupling multinuclear RF coils. 2014;72(2):584–590.
21. Dabirzadeh A, McDougall MP. Trap Design for Insertable Second-Nuclei Radiofrequency Coils for Magnetic Resonance Imaging and Spectroscopy. Concepts in Magnetic Resonance Part B (Magnetic Resonance Engineering),. 2009;35B(3):121–132.
22. Shajan G, Hoffmann J, Budde J, Adriany G, Ugurbil K, Pohmann R. Design and evaluation of an RF front-end for 9.4 T human MRI. Magn Reson Med 2011;66(2):596–604. [PubMed: 21381102]
23. Roemer PB, Edelstein WA, Hayes CE, Souza SP, Mueller OM. The NMR phased array. Magn Reson Med 1990;16(2):192–225. [PubMed: 2266841]
24. Alagappan V, Nistler J, Adalsteinsson E, et al. Degenerate mode band-pass birdcage coil for accelerated parallel excitation. Magn Reson Med 2007;57(6):1148–1158. [PubMed: 17534905]
25. Lin F, Kwong K, Huang I, Belliveau J, Wald L. Degenerate mode birdcage volume coil for sensitivity-encoded imaging. Magn Reson Med 2003;50:1107–1111. [PubMed: 14587023]

26. Frahm J, Merboldt K-D, Hänicke W. Localized proton spectroscopy using stimulated echoes. Journal of Magnetic Resonance (1969). 1987;72(3):502–508.
27. Pipe JG, Zwart NR, Aboussouan EA, Robison RK, Devaraj A, Johnson KO. A new design and rationale for 3D orthogonally oversampled k-space trajectories. Magn Reson Med 2011;66(5): 1303–1311. [PubMed: 21469190]
28. Madelin G, Kline R, Walvick R, Regatte RR. A method for estimating intracellular sodium concentration and extracellular volume fraction in brain in vivo using sodium magnetic resonance imaging. Sci Rep 2014;4:4763. [PubMed: 24755879]
29. Kellman P, McVeigh ER. Image reconstruction in SNR units: a general method for SNR measurement. Magn Reson Med. 2005;54(6):1439–1447. [PubMed: 16261576]
30. Fautz HP, Vogel M, Gross P, Kerr A, Zhu Y. B1 mapping of coil arrays for parallel transmission ISMRM; 2008; Toronto, Ontario.
31. Brown R, Madelin G, Lattanzi R, et al. Design of a nested eight-channel sodium and four-channel proton coil for 7T knee imaging. Magn Reson Med 2013;70(1):259–268. [PubMed: 22887123]
32. Kaggie JD, Hadley JR, Badal J, et al. A 3 T sodium and proton composite array breast coil. Magn Reson Med 2014;71(6):2231–2242. [PubMed: 24105740]
33. Moon CH, Kim J-H, Zhao T, Bae KT. Quantitative 23Na MRI of human knee cartilage using dual-tuned 1H/23Na transceiver array radiofrequency coil at 7 tesla. 2013;38(5):1063–1072.
34. Shajan G, Mirkes C, Buckenmaier K, Hoffmann J, Pohmann R, Scheffler K. Three-layered radio frequency coil arrangement for sodium MRI of the human brain at 9.4 Tesla. Magn Reson Med 2015.

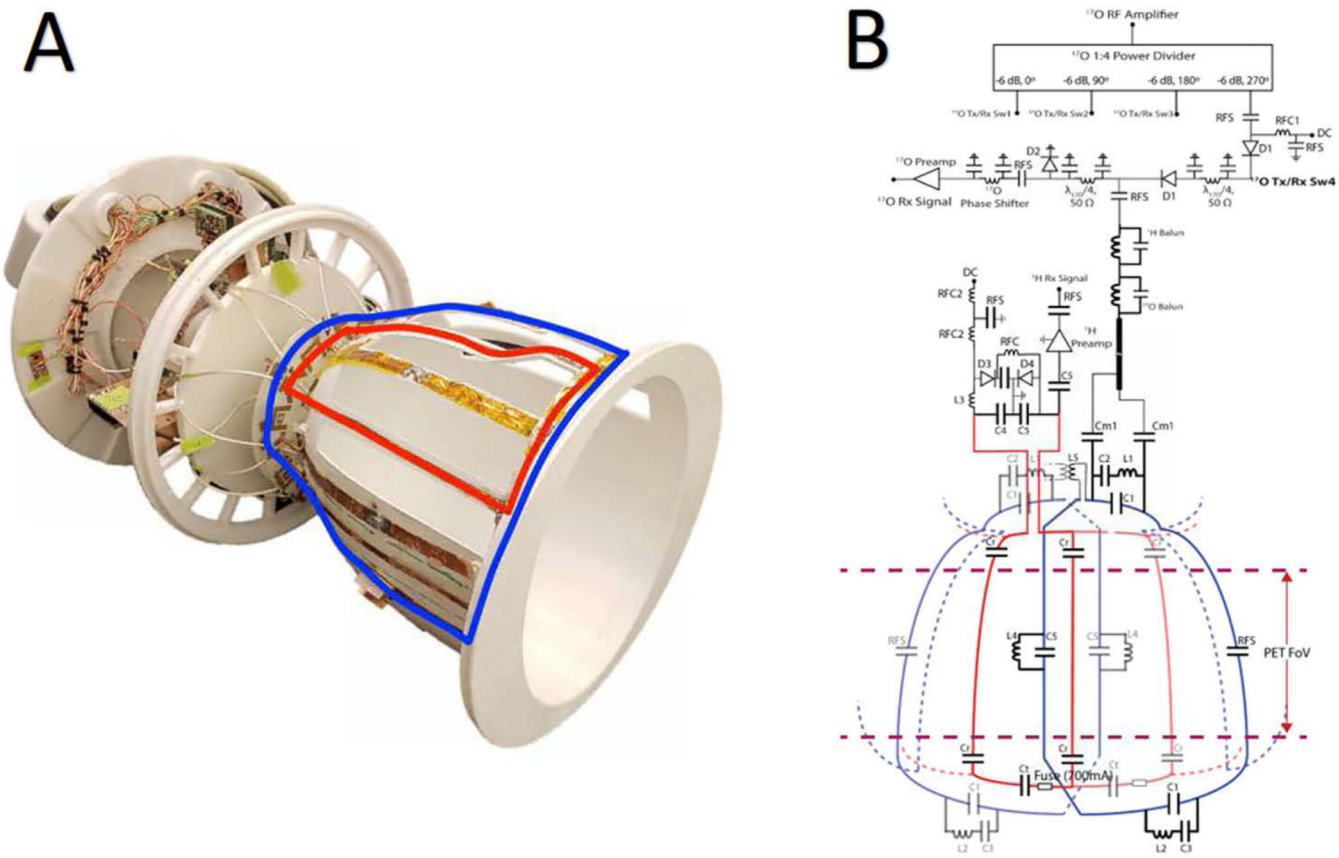

Figure 1.

Photograph of the $^{17}O/^{1}H$ array without protective cover (A). The blue and red overlays indicate the contour of individual ^{17}O and ^{1}H coils, respectively. The interface components, including preamplifiers, power dividers, and transmit/receive switches, are located superior to the coils to reduce PET attenuation in future MR/PET studies.

Schematic diagram of the $^{17}O/^{1}H$ coil array and interface (B). ^{17}O coils are represented in blue and ^{1}H coils in red. For simplicity one ^{17}O and ^{1}H coil are highlighted. For both the ^{17}O and ^{1}H arrays the status of the DC bias is forward in transmit mode and reverse in receive mode. In receive mode the diodes D1 provide isolation between the RF amplifier and preamplifiers. The diode D2 provides isolation between the RF amplifier and the preamplifier in transmit mode. During proton body coil excitation the diode D3 along with L3 and C4 forms the detuning circuit, the diode D4 provides protection for the preamplifier. Typical component values are C1=47 pF, C2=200pF, C3=300pF, C4 =15pF, C5=27pF, Cm1=180pF, Cr=18pF, Ct = 2–15 pF, L1= 38nH, L2 = 80nH, L3= 105 nH and L4 = 60 nH, L5 = 230 nH, RFC1 = 10μH, RFC2 =2.2μH, RFS =1000pF.

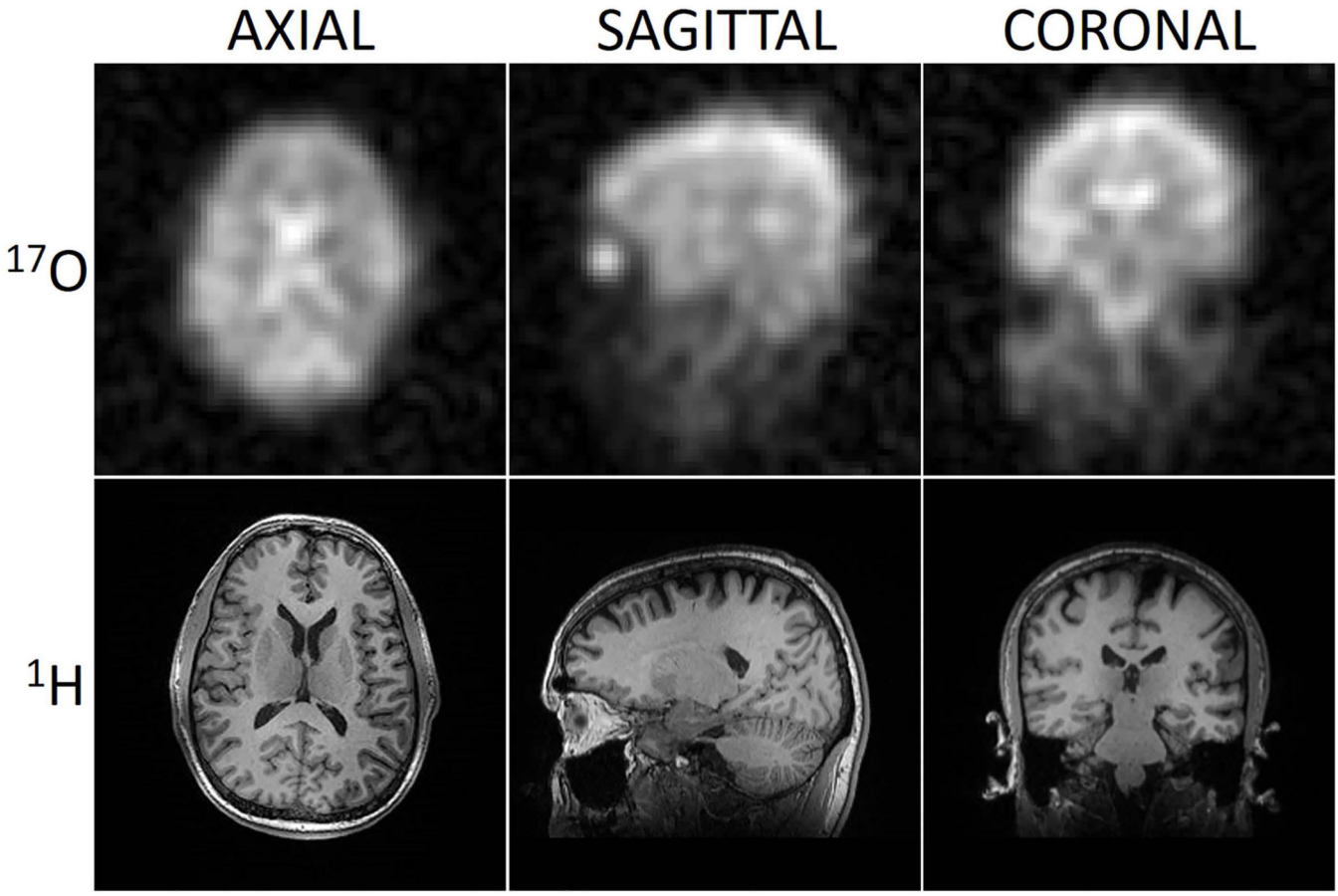

Figure 2.

In vivo FLORET ^{17}O images (top row) and co-registered MPRAGE ^{1}H images (bottom row) acquired using the $^{17}O/^{1}H$ array. ^{17}O FLORET images reflect the underlying water pool with greatest intensity in the ventricular system, cisterns/sulci, grey matter and intraocular vitreous. The ^{1}H MPRAGE images demonstrate excellent T_1 contrast in the whole brain.

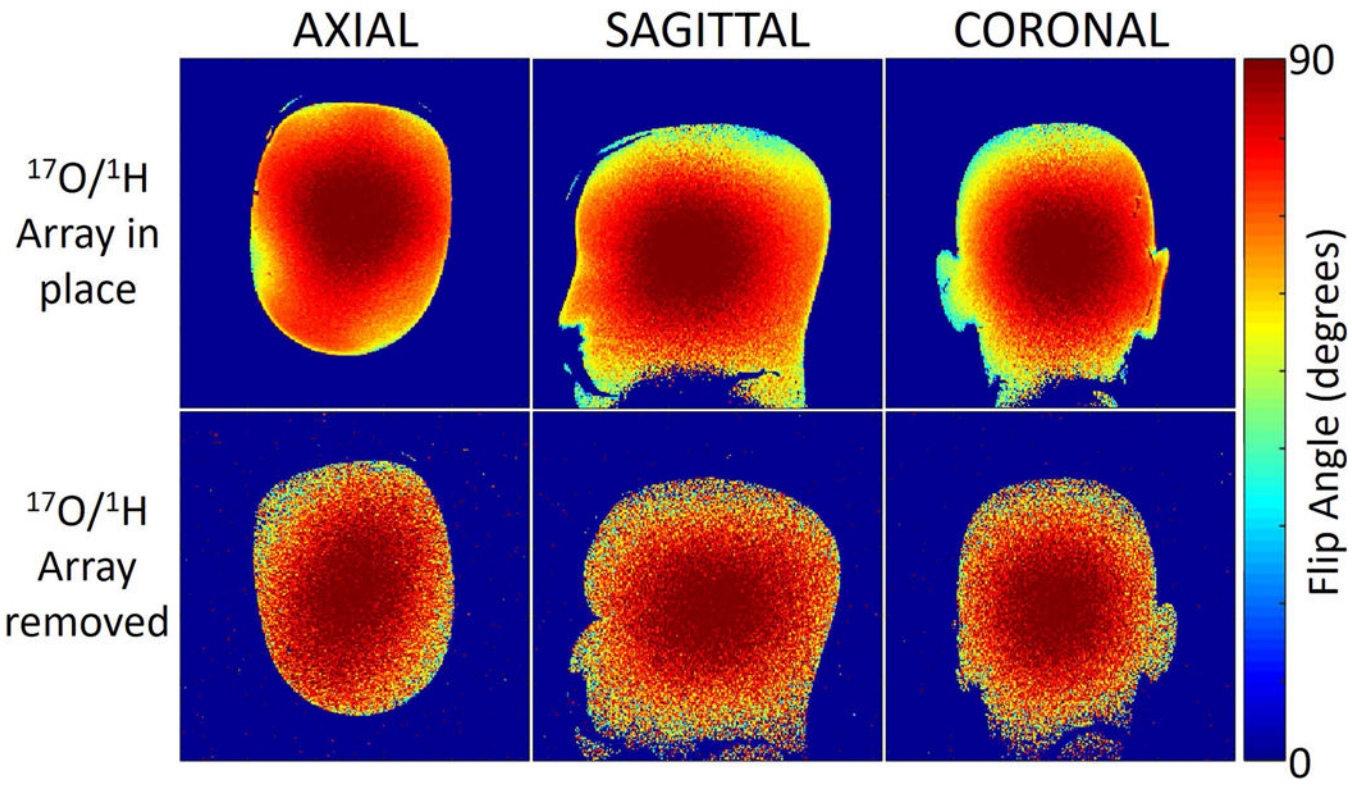

Figure 3.

^{1}H flip angle maps measured in a head shaped phantom with and without the $^{17}O/^{1}H$ array. The flip angle maps show that the $^{17}O/^{1}H$ array caused minimal distortion to the transmit field produced by the system body coil. The low SNR on the bottom row is attributed to the use of system body coil for signal reception.

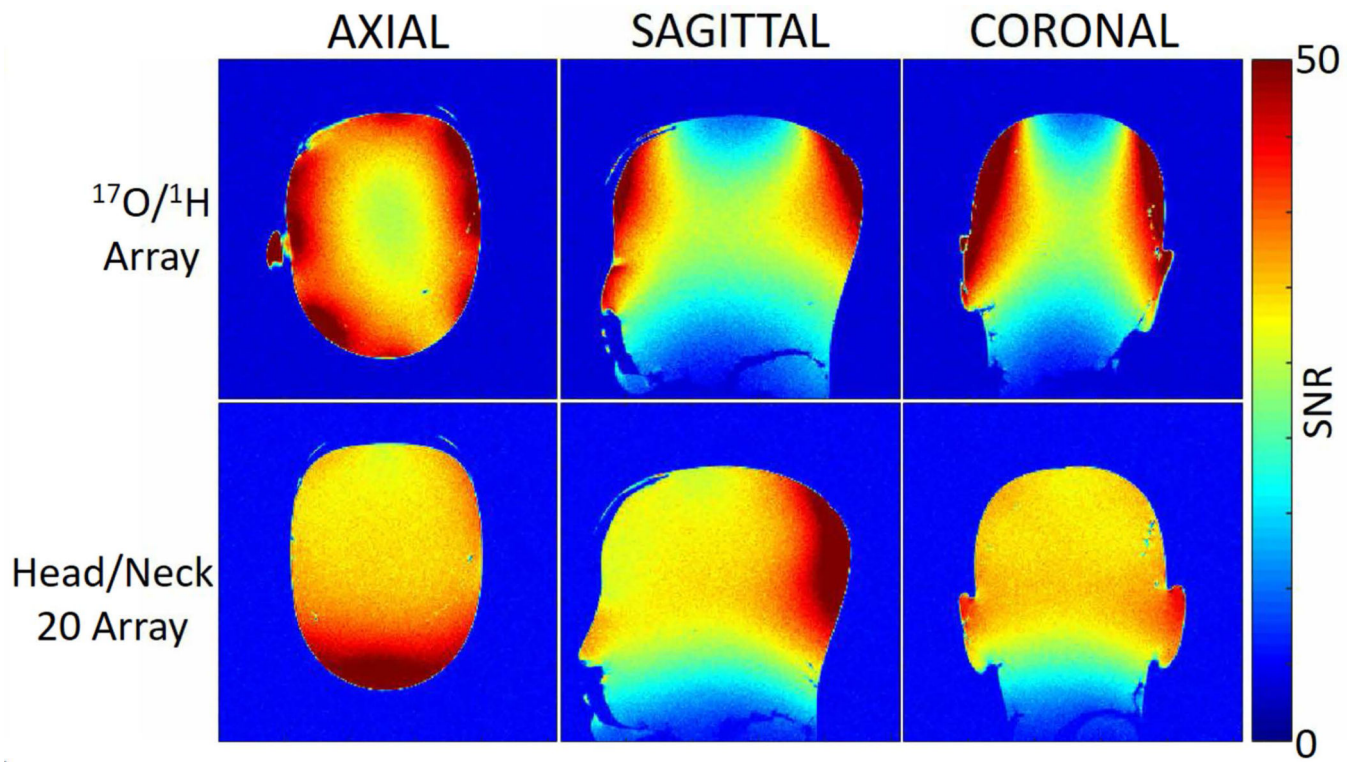

Figure 4.

^{1}H SNR maps measured in a head shaped phantom show that the commercial Head/Neck 20 array outperforms the $^{17}O/^{1}H$ array by 20% at the center of the phantom.

Table 1

Q measurements on candidate ^{17}O coils with various apertures and tuning components. The coil length was fixed at 27 cm, with apertures to emulate a single coil in a 4 (90°) or 8 channel (45°) array. The coil with 90° aperture and 2 distributed capacitors represents the baseline (row 1), while the others show compromised performance primarily due to increased capacitor loss (row 2) or reduced coil-to-sample coupling (row 3). This information motivated the implemented design (row 4), in which the aperture provided sufficient coil-to-sample coupling, while loss due to ^{1}H blocking circuits was considered a necessary penalty to enable 1H body coil excitation.

Aperture	Number of Distributed capacitors	Unloaded Q Q_{un}	Loaded Q Q_l	Ratio Q_{un}/Q_l
90°	2	420	190	2.21
90°	4	320	180	1.78
45°	2	285	170	1.68
90°	1 first-order and 2 second-order blocking circuits	320	180	1.78